

## Spin polarons in $\text{La}_{1-x}\text{Sr}_x\text{CoO}_3$ single crystals

R. X. Smith,<sup>1</sup> M. J. R. Hoch,<sup>1</sup> P. L. Kuhns,<sup>1</sup> W. G. Moulton,<sup>1</sup> A. P. Reyes,<sup>1</sup> G. S. Boebinger,<sup>1</sup>  
J. Mitchell,<sup>2</sup> and C. Leighton<sup>3</sup>

<sup>1</sup>National High Magnetic Field Laboratory, Florida State University, Tallahassee, Florida 32310, USA

<sup>2</sup>Materials Science Division, Argonne National Laboratory, Argonne, Illinois 60439, USA

<sup>3</sup>Department of Chemical Engineering and Materials Science, University of Minnesota, Minneapolis, Minnesota 55455, USA

(Received 6 August 2008; published 12 September 2008)

Nanoscale inhomogeneity in  $\text{La}_{1-x}\text{Sr}_x\text{CoO}_3$  has been investigated in single-crystal samples for  $0.05 \leq x \leq 0.30$  using  $^{139}\text{La}$  and  $^{59}\text{Co}$  NMR to probe local magnetization. In contrast to polycrystalline samples, single crystals exhibit ferromagnetism only above the metal-insulator critical concentration  $x_C=0.17$ . However, over the entire doping range, the single crystals exhibit an unusually broad and asymmetric distribution of hyperfine fields, evidencing (local) spin-polaron formation that persists to temperatures as high as 200 K, well above the glass transition reported previously from bulk magnetization. Above  $x_C$  the asymmetry decreases rapidly with increasing doping as polarons overlap to give rise to long-range ferromagnetism. A modified phase diagram is presented. The key features of the data are reproduced by a simple model in which Sr dopants trigger spin-polaron formation, a physical picture first proposed by de Gennes [Phys. Rev. **118**, 141 (1960)].

DOI: [10.1103/PhysRevB.78.092201](https://doi.org/10.1103/PhysRevB.78.092201)

PACS number(s): 71.30.+h, 75.30.Kz, 76.60.Jx

The occurrence of nanoscale phase separation has been established in transition-metal oxides, particularly the cuprates and manganites,<sup>1,2</sup> and is very important in determining the magnetic and transport properties of these systems.<sup>3–5</sup> In particular, phase separation has been suggested as a key to understanding the large magnetoresistance in cobaltites and manganites. The phase diagram for  $\text{La}_{1-x}\text{Sr}_x\text{CoO}_3$  (Refs. 6–8) has a metal-insulator (MI) transition at the critical concentration  $x_C=0.17$  with long-range ferromagnetism occurring in the metallic phase ( $x \geq 0.17$ ) below the Curie temperature  $T_C$ . Phase separation in  $\text{La}_{1-x}\text{Sr}_x\text{CoO}_3$  has been observed in sintered polycrystalline samples in the range  $0.10 \leq x \leq 0.30$ .<sup>9–14</sup> For  $x < x_C$  a droplet model involving ferromagnetic (FM) clusters in a nonferromagnetic matrix has been proposed to account for the large magnetoresistance and other interesting properties.<sup>7,8,14–17</sup>

Recent neutron-scattering<sup>15</sup> and bulk magnetization<sup>16</sup> experiments on single-crystal samples, however, show that phase separation in single crystals occurs over a much narrower range ( $0.17 \leq x < 0.30$ ) than in polycrystalline samples. NMR provides a powerful means for detecting local inhomogeneities in magnetic materials from the local hyperfine (internal magnetic) field distribution. Using  $^{139}\text{La}$  and  $^{59}\text{Co}$  NMR, we find internal magnetic-field distributions inconsistent with the simple droplet model described above and consistent with a model first proposed by de Gennes,<sup>18</sup> where an inhomogeneous system is driven by the nucleation of spin polarons at each Sr ion.

In  $\text{La}_{1-x}\text{Sr}_x\text{CoO}_3$ , coupling between pairs of Co ions in different valence states is due to the double-exchange (DE) mechanism<sup>19</sup> involving  $\sigma^*$  ( $e_g$  parentage) electrons in the hole-doped regions. The driving mechanism determining the internal field distribution in the cobaltites is not well understood but involves competing effects, including DE interactions, Coulomb energy, and Jahn-Teller distortions, either locally or over an extended range.<sup>20–23</sup> Small-angle neutron-scattering experiments on polycrystalline<sup>14</sup>  $\text{La}_{1-x}\text{Sr}_x\text{CoO}_3$  and neutron scattering on single crystals<sup>15</sup> show that the FM

correlation length  $\xi$  increases with increasing  $x$  as the MI transition is crossed. Recent elastic neutron-scattering measurements<sup>24</sup> show that the FM regions coexist with an incommensurate spin structure arising from local order of  $\text{Co}^{3+}\text{-Co}^{4+}$  clusters.

The present work has applied NMR to a set of floating-zone grown single-crystal  $\text{La}_{1-x}\text{Sr}_x\text{CoO}_3$  samples with  $x$  values in the range 0.05–0.30 as used in a recent investigation of transport and magnetic properties.<sup>14,16</sup> The compositional uniformity of the single crystals was verified using scanning transmission electron microscopy. All samples were crushed to a grain size of  $\sim 20$   $\mu\text{m}$  to overcome rf skin-depth problems. The spectra were recorded in the range 2–300 K, following field cooling in 10 T, by integrating the spin echo at fixed frequency while sweeping the magnetic field over the range 10–15 T. The spectral shape is independent of (i) the sample cooling protocol in either high field or zero field (ZF) and (ii) the applied magnetic field over the entire experimental range of 6–15 T. Magnetoresistance measurements show no evidence of a field-induced MI transition.

$^{139}\text{La}$  NMR spectra in  $\text{La}_{1-x}\text{Sr}_x\text{CoO}_3$  exhibit down-field shifts from the bare nucleus value, proportional to the local magnetization, and thus map the internal magnetic-field distribution. The  $^{139}\text{La}$  ( $^{139}\gamma/2\pi=6.0146$  MHz/T) resonance field corresponding to the measuring frequency of 84.2 MHz is 14 T as determined in an  $x=0$  sample at 4 K. Figures 1 and 2(a) show our  $^{139}\text{La}$  spectra (open circles) for our single-crystal samples as a function of  $T$  and  $x$ . The NMR spectra are broad and in general asymmetric, corresponding to a continuous distribution of hyperfine fields at the La sites, and stand in stark contrast to the two-peak spectra of the sintered polycrystalline samples<sup>12</sup> [shown as heavy red lines in Fig. 2(a) for  $x=0.10, 0.18,$  and  $0.30$ ].

All  $^{139}\text{La}$  spectra in Figs. 1 and 2(a) can be well fit (blue lines) using a skewed Gaussian (skew—normal) function that uses three independent parameters (center field  $\langle H_{\text{hf}} \rangle$ , width  $\Delta H_{\text{hf}}$ , and skew  $\alpha$ ). The lack of structure in these spectra does not justify fitting with multiple Gaussians. The form used is

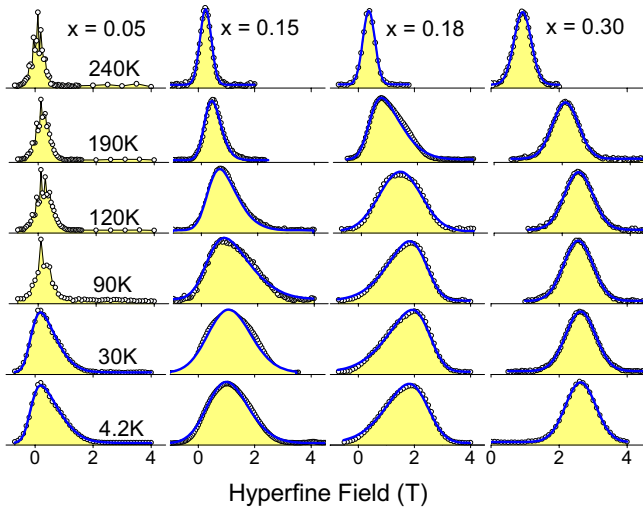


FIG. 1. (Color online)  $^{139}\text{La}$  NMR field-sweep spectra (open circles) for single-crystal  $\text{La}_{1-x}\text{Sr}_x\text{CoO}_3$  at 84.2 MHz show the distribution of the hyperfine field at La sites for selected  $x$  and  $T$ . The heavy blue lines are fits using the skew-normal distribution described in text.

$$F(\alpha, \langle H_{\text{hf}} \rangle, \Delta H_{\text{hf}}) = G(\langle H_{\text{hf}} \rangle, \Delta H_{\text{hf}}) \Phi(\alpha, \langle H_{\text{hf}} \rangle)$$

with

$$\Phi(\alpha, \langle H_{\text{hf}} \rangle) = 1 + \int_0^{\alpha \langle H_{\text{hf}} \rangle} G(H', \Delta H') dH' = 1 + \text{erf}(\alpha, \langle H_{\text{hf}} \rangle),$$

where  $G(\langle H_{\text{hf}} \rangle, \Delta H_{\text{hf}})$  is a Gaussian,  $\text{erf}(\alpha, \langle H_{\text{hf}} \rangle)$  is the error function and  $\alpha$  is an adjustable skew parameter that may be positive or negative.  $\Phi(\alpha, \langle H_{\text{hf}} \rangle)$  acts to skew the line shape such that when  $\alpha=0$  the line shape is Gaussian and as  $\alpha$  increases the line shape approaches half Gaussian. The closed circles in Fig. 2(b) are the fitting parameters  $\langle H_{\text{hf}} \rangle$ ,  $\Delta H_{\text{hf}}$ , and  $\alpha$  obtained for the 4 K spectra as a function of  $x$ . Note that the skew parameter, a measure of the asymmetry of the distribution, changes sign at  $x_C=0.17$  as the spectral weight shifts from small  $\langle H_{\text{hf}} \rangle$  to large  $\langle H_{\text{hf}} \rangle$  (Fig. 2). Furthermore for all  $x > 0.15$ ,  $\langle H_{\text{hf}} \rangle \sim 2.6$  T is consistent with the onset of long-range FM order. ZF  $^{59}\text{Co}$  NMR tests this interpretation as it is sensitive only to the presence of FM; the 0.15 sample shows no evidence of FM regions whereas the 0.18 and 0.30 samples give broad ( $\sim 10$  T) ZF spectra. We find that this signature of FM in single crystals and sintered polycrystalline samples<sup>11,25</sup> is identical; however, in the single crystals, long-range FM appears only for  $x \geq 0.17$  and is negligible at lower dopings; specifically, the FM volume fraction is less than  $\sim 1\%$  for  $x \leq 0.15$ .

At the highest doping of  $x=0.3$ , the spectrum is well fit using a single symmetric Gaussian for which the down-field shift of 2.6 T corresponds to a frequency shift of 15.6 MHz. This is in quantitative agreement with the transferred hyperfine interaction obtained in ZF NMR experiments<sup>26</sup> as well as the previous  $^{139}\text{La}$  FM shift found in sintered  $\text{La}_{1-x}\text{Sr}_x\text{CoO}_3$ .<sup>12</sup> We therefore identify the data at  $x=0.3$  as fully FM. Turning to the temperature dependence of the

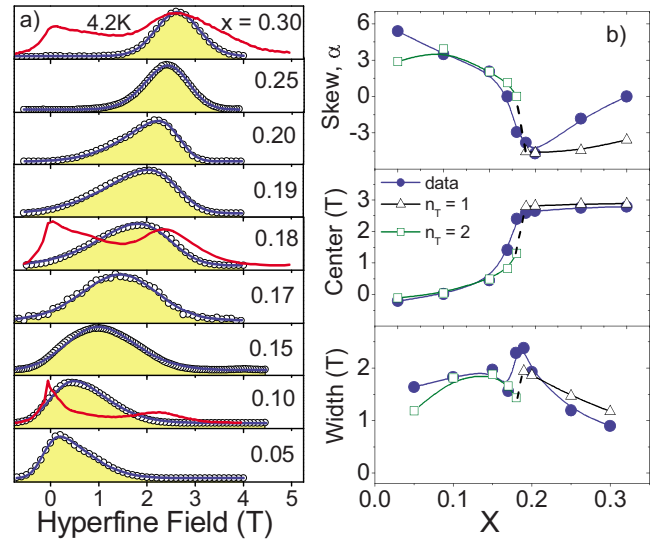


FIG. 2. (Color online) (a) Doping dependence of spectra (open circles) at  $T=4.2$  K for all doping levels studied:  $0.05 \leq x \leq 0.30$  at 4.2K. The skew-normal fits are indicated by the heavy blue lines. Polycrystalline spectra (heavy red lines) are shown for  $x=0.10$ , 0.18, and 0.30. Figure 2(b) shows the skew-normal fitting parameters (circles) from the fits to the  $^{139}\text{La}$  NMR spectra of  $\text{La}_{1-x}\text{Sr}_x\text{CoO}_3$  at  $T=4.2$  K [Fig. 2(a)]. Center field  $\langle H_{\text{hf}} \rangle$ , width,  $\Delta H_{\text{hf}}$  and skew  $\alpha$  are defined in text, and the solid lines are guides to the eye. The open squares (triangles) are the skew-normal parameters for the statistical inhomogeneity model with a threshold value  $n_T=2$  ( $n_T=1$ ), discussed in text.

NMR spectra, Fig. 3 plots  $\langle H_{\text{hf}} \rangle$ ,  $\Delta H_{\text{hf}}$ , and  $\alpha$  as a function of  $T$  for the  $x=0.05$ , 0.15, 0.18, 0.19, 0.25, and 0.30 samples.  $\langle H_{\text{hf}} \rangle$  for  $x=0.25$  and 0.30 shows significant shift ( $\sim 1.5$  T) above  $T_C$  with little (0.25) or no (0.30) skew. High magnetic fields smear magnetic transitions, however, extrapolating the  $x=0.30$   $\langle H_{\text{hf}} \rangle$  curve shows  $\langle H_{\text{hf}} \rangle$  reaching 0 T at  $\sim 340$  K, very close to the formation temperature of magnetic clusters seen in Ref. 8. Both  $x=0.18$  and 0.19 show much smaller  $\langle H_{\text{hf}} \rangle$  values ( $\sim 0.25$  T) above  $T_C$  yet both exhibit sudden large increases in  $\langle H_{\text{hf}} \rangle$  at  $T_C$  unlike  $x=0.25$  and 0.30, which appear unaffected. For both  $x=0.18$  and 0.19,  $\alpha$  continuously increases with decreasing  $T$  peaking at  $T_C$  before decreasing and changing sign. Interestingly, lowering the temperature further reveals a local maximum in  $\langle H_{\text{hf}} \rangle$  and local minimum in  $\alpha$  corresponding to a shift in spectral weight to weaker magnetic regions. This shift in spectral weight is more pronounced as doping decreases and persists below the MI transition to  $x=0.15$ , where it is accompanied by a local minimum in  $\Delta H_{\text{hf}}$ . Comparing the temperatures at which these shifts in spectral weights occur with the appearance of the incommensurate spin structures seen in Ref. 24 reveals an interesting correlation. Both  $x=0.05$  and 0.15 spectra exhibit skew (presence of polarons) at temperatures much higher than the spin-glass freezing temperature  $T_g$ . For comparison purposes, the low applied field glassy transition temperatures  $T_g$  or (for  $x > x_C$ )  $T_C$  are indicated for each  $x$  value. Spin-glass behavior has been reported<sup>27</sup> but  $\langle H_{\text{hf}} \rangle$  is much larger here than expected for a conventional spin glass. The peaks in  $x=0.05$  spectra above 30 K are resolved electric quadrupolar satellites. For  $x \geq 0.15$  the satellites are smeared out by

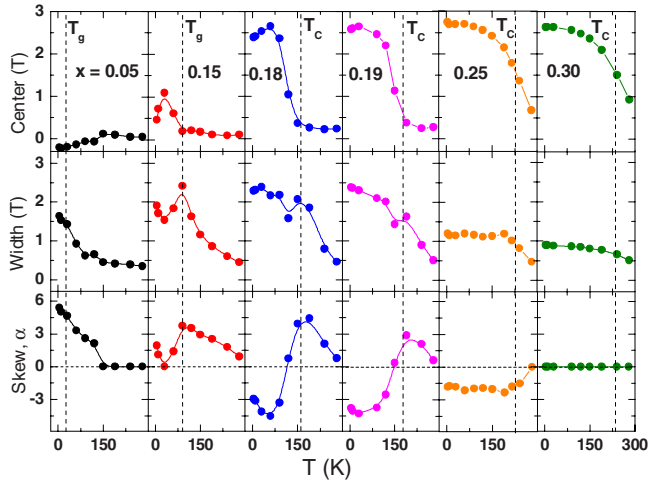


FIG. 3. (Color online) Temperature dependence of the skew-normal fitting parameters for  $x=0.05, 0.15, 0.18, 0.19, 0.25,$  and  $0.30$  samples, for which the solid lines are guides to the eye. The vertical dotted lines show the transition temperatures  $T_g$  and  $T_c$  from low-field measurements (Ref. 16).

hyperfine fields for all measured temperatures.

For near-cubic  $\text{La}_{1-x}\text{Sr}_x\text{CoO}_3$  the dominant transferred hyperfine interaction at a La nuclear site is the isotropic part given by the Hamiltonian  $H = \hbar \sum A_i I \cdot S_i$  with  $I = 7/2$  as the nuclear spin,  $S_i$  as the coupled nearest-neighbor (NN) electron spins at Co ion sites  $i$ , and  $A_i$  as the corresponding transferred hyperfine coupling constant produced by orbital hybridization. For this FM system in an applied magnetic field  $H_0$ , the nuclear resonance frequency obtained by summing over the eight nearest neighbors is  $f = (\gamma_I/2\pi)[H_0 + 8Ag\mu_B \langle S \rangle_{\text{loc}}] = (\gamma_I/2\pi)[H_0 + H_I]$  with  $\langle S \rangle_{\text{loc}}$  as the average for local spins  $S_i$  on the neighboring Co ions and  $A$  (in units of  $T/\mu_B$ ) as the average hyperfine coupling.

We propose a *statistical inhomogeneity model* that accounts for the observed skew-normal NMR spectra by considering a  $180 \times 180 \times 180$  lattice with random Sr doping. The model assumes that small polarons form in cells containing Sr ions with mobile holes shared by the eight NN Co ions as proposed by de Gennes.<sup>18</sup> The polarization  $\langle S \rangle$  of a given Co ion is proportional to the number  $n$  of NN  $\text{Sr}^{2+}$  ions. We fix  $A$  to match the measured hyperfine field of 2.5 T (per the  $x=0.30$  spectra at 4.2 K), and assume that  $A$  is independent of  $i$  and  $x$ . This model reproduces the following features of the data: (1) broad and skewed hyperfine field distribution, (2) the crossover from positive to negative skewness at an intermediate value of  $x$ , and (3) the anomaly in the linewidth at the crossover [Fig. 3(c)]. Within this model, the data indicate that a Co ion is fully polarized for  $n \geq 3$ ; however, this model finds a crossover at  $x=0.23$  that is less sudden than the observed transition.

The model described above cannot capture the transfer of polarization between Co ions via mobile holes because each hole is confined to a single unit cell. In the actual material, hole mobility will increase as nearest-neighbor Co ions become aligned. We find improved agreement with the data of Fig. 2(b) (magnitude of the fit parameters and a sharp transition at  $x=0.18$ ) by mimicking hole motion in an *ad hoc*

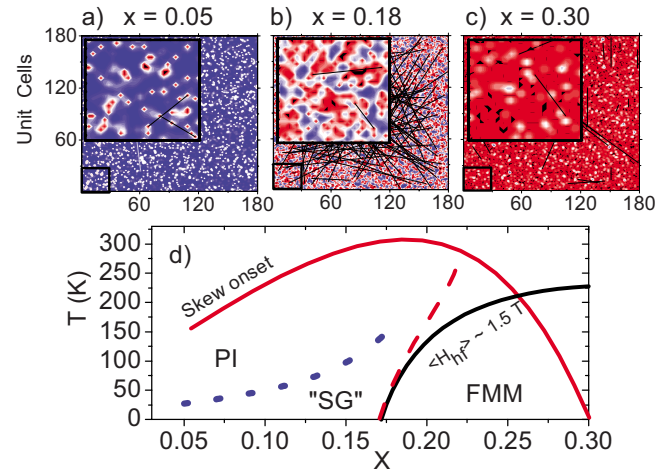


FIG. 4. (Color online) (a)–(c) Hyperfine field distribution from the model for  $x=0.05, 0.18,$  and  $0.30$ , respectively. The magnified insets ( $30 \times 30$  unit cells) show the random Sr-dopant sites (black) and the continuous nature of the field distribution, consistent with the NMR data of Figs. 1–3. (d) The dark solid line marks the boundary below which the measured  $\langle H_{\text{hf}} \rangle$  is greater than 1.5 T, in good agreement with the ferromagnetic metal (FMM) phase reported from transport and magnetization (Ref. 16). The “skew onset” line indicates the strikingly large region of the phase diagram exhibiting skewed spectra in Figs. 1–3. The dashed line marks the crossover from positive to negative skew, which matches the insulator-to-metal transition from transport data (Ref. 16) at low temperatures. The dotted line indicates the spin-glass (SG) region from Ref. 16, which lies outside our polaron model.

manner: (1) We identify every connected region of Co ions within which each Co has *at least* a threshold number ( $n_T$ ) of nearest-neighbor Sr. (2) We find the single Co ion in each region with the highest polarization and assign that value to *all* of the Co ions within that region. The open squares in Fig. 2(b) are the results from the model using a threshold value  $n_T=2$ , which fixes  $x_C=0.18$  and shows quantitative agreement for all  $x < x_C$ . Quantitative agreement for  $x > x_C$  requires  $n_T=1$  (consistent with enhanced hole mobility), although the model leaves unexplained why the value of  $n_T$  would change across the transition. We emphasize that the *statistical inhomogeneity model* captures the salient features of the data even without the *ad hoc* addition of the unconstrained free parameter  $n_T$ .

Two-dimensional slices of the model lattice are shown in Figs. 4(a)–4(c) for  $x=0.05, 0.18,$  and  $0.30$ , respectively. The slices are  $180 \times 180$  unit cells with the insets showing  $30 \times 30$  unit cells. The color scale is a mapping of the La hyperfine field with dark red being the saturated ferromagnetic moment and dark blue being zero internal field. The continuous distribution of the polarization is consistent with the data of Figs. 1–3 and is distinctly inconsistent with a simple two-phase model in which nanoscale regions are either paramagnetic insulator or FM metal (FMM). Figure 4(d) shows a modified phase diagram that captures the primary features of the NMR data: (1) a crossover from positive to negative skewness that corresponds to the MI transition in the low-temperature limit; (2) a region for which  $\langle H_{\text{hf}} \rangle \geq 1.5$  T that matches the FMM phase found in transport and

magnetization;<sup>8</sup> and, most strikingly, (3) a “skew onset” line (below which the NMR spectra are asymmetric) that is located at *much* higher temperatures than the previously reported glassy transition (dotted line from Ref. 16), which evidences the existence of polarons at extremely high temperatures across the entire phase diagram, even for  $x < x_C$ .

In conclusion broad skew-normal distributions in the hyperfine field reveal the occurrence of nanoscale inhomogeneity and polaronic behavior in single-crystal  $\text{La}_{1-x}\text{Sr}_x\text{CoO}_3$  over a wide range in the  $x$ - $T$  plane. A simple model based on

random Sr dopants provides a physical picture for the observed continuous distribution of hyperfine fields from weakly polarized to highly polarized regions.

Financial support by the NSF under Cooperative Agreement No. DMR-0234125 and by the State of Florida is gratefully acknowledged. Work at UMN was supported by DOE (Grant No. DE-FG02-06ER46275) and NSF (Grant No. DMR 05099666). We thank S. von Molnar and P. B. Littlewood for their helpful polarizing discussions.

- 
- <sup>1</sup>E. Dagotto, *Nanoscale Phase Separation and Colossal Magnetoresistance*, Solid-State Sciences Series (Springer-Verlag, Berlin, 2002).
- <sup>2</sup>P. A. Lee, N. Nagaosa, and X.-G. Wen, *Rev. Mod. Phys.* **78**, 17 (2006).
- <sup>3</sup>P. Y. Chan, N. Goldenfeld, and M. Salamon, *Phys. Rev. Lett.* **97**, 137201 (2006).
- <sup>4</sup>V. B. Shenoy, T. Gupta, H. R. Krishnamurthy, and T. V. Ramakrishnan, *Phys. Rev. Lett.* **98**, 097201 (2007).
- <sup>5</sup>G. Bouzerar, and O. Cépas, *Phys. Rev. B* **76**, 020401(R) (2007).
- <sup>6</sup>J. Wu and C. Leighton, *Phys. Rev. B* **67**, 174408 (2003).
- <sup>7</sup>M. Itoh, I. Natori, S. Kubota, and K. Motoya, *J. Phys. Soc. Jpn.* **63**, 1486 (1994).
- <sup>8</sup>C. He, M. A. Torija, J. Wu, J. W. Lynn, H. Zheng, J. F. Mitchell, and C. Leighton, *Phys. Rev. B* **76**, 014401 (2007).
- <sup>9</sup>R. Caciuffo, D. Rinaldi, G. Barucca, J. Mira, J. Rivas, M. A. Señarís-Rodríguez, P. G. Radaelli, D. Fiorani, and J. B. Goodenough, *Phys. Rev. B* **59**, 1068 (1999).
- <sup>10</sup>J. Mira, J. Rivas, R. D. Sánchez, M. A. Señarís-Rodríguez, D. Fiorani, D. Rinaldi, and R. Caciuffo, *J. Appl. Phys.* **81**, 5753 (1997).
- <sup>11</sup>P. L. Kuhns, M. J. R. Hoch, W. G. Moulton, A. P. Reyes, J. Wu, and C. Leighton, *Phys. Rev. Lett.* **91**, 127202 (2003).
- <sup>12</sup>M. J. R. Hoch, P. L. Kuhns, W. G. Moulton, A. P. Reyes, J. Lu, J. Wu, and C. Leighton, *Phys. Rev. B* **70**, 174443 (2004).
- <sup>13</sup>J. Wu, H. Zheng, J. F. Mitchell and C. Leighton, *Phys. Rev. B* **73**, 020404(R) (2006).
- <sup>14</sup>J. Wu, J. W. Lynn, C. J. Glinka, J. Burley, H. Zheng, J. F. Mitchell, and C. Leighton, *Phys. Rev. Lett.* **94**, 037201 (2005).
- <sup>15</sup>D. Phelan, D. Louca, S. Rosenkranz, S.-H. Lee, Y. Qiu, P. J. Chupas, R. Osborn, H. Zheng, J. F. Mitchell, J. R. D. Copley, J. L. Sarrao, and Y. Moritomo, *Phys. Rev. Lett.* **96**, 027201 (2006).
- <sup>16</sup>H. M. Aarbhogh, J. Wu, L. Wang, H. Zheng, J. F. Mitchell, and C. Leighton, *Phys. Rev. B* **74**, 134408 (2006).
- <sup>17</sup>Y. K. Tang, Y. Sun, and Z. H. Cheng, *Phys. Rev. B* **73**, 012409 (2006).
- <sup>18</sup>P.-G. de Gennes, *Phys. Rev.* **118**, 141 (1960).
- <sup>19</sup>K. Kubo and N. Ohata, *J. Phys. Soc. Jpn.* **33**, 21 (1972).
- <sup>20</sup>G. C. Milward, M. J. Calderón, and P. B. Littlewood, *Nature (London)* **433**, 607 (2005).
- <sup>21</sup>K. I. Kugel, A. L. Rakhmanov, and A. O. Sboychakov, *Phys. Rev. Lett.* **95**, 267210 (2005).
- <sup>22</sup>D. Louca, J. L. Sarrao, J. D. Thompson, H. Röder, and G. H. Kwei, *Phys. Rev. B* **60**, 10378 (1999).
- <sup>23</sup>D. Louca and J. L. Sarrao, *Phys. Rev. Lett.* **91**, 155501 (2003).
- <sup>24</sup>D. Phelan, D. Louca, K. Kamazawa, S. H. Lee, S. Rosenkranz, M. F. Hundley, J. F. Mitchell, Y. Motome, S. N. Ancona, and Y. Moritomo, *Phys. Rev. Lett.* **97**, 235501 (2006).
- <sup>25</sup>M. J. R. Hoch, P. L. Kuhns, W. G. Moulton, A. P. Reyes, M. A. Torija, J. F. Mitchell, and C. Leighton, *Phys. Rev. B* **75**, 104421 (2007).
- <sup>26</sup>M. Itoh and I. Natori, *J. Phys. Soc. Jpn.* **64**, 970 (1995).
- <sup>27</sup>J. M. D. Coey, M. Viret, and S. von Molnár, *Adv. Phys.* **48**, 167 (1999).